Plasma and ions - current measurements and theoretical models

J. Kellerer F. Spanier

March 19, 2019

1 Introduction

The KATRIN experiment is designed to achieve a very high precision for the neutrino mass measurement. The desired precision can only be reached when plasma effects are accounted for. Unfortunately in-situ plasma measurements are not available and theoretical models have to make a large number of a priori assumptions and are interlinked to a very high degree (e.g., plasma models require ion distributions as input, but the ion distributions are depending on plasma parameters).

With the advent of first tritium more and more measurements are available that shed light on plasma and ion conditions within the KATRIN experiment. Unfortunately only derived quantities are available from the measurement.

This document serves as a starting point for the discussion of the connection of plasma theory and recent measurements. An important point is to identify the a priori assumptions, the available simulations and the implications of measurements on them.

1.1 Naming of variables

The source section has many different regions with entirely different properties. So the following naming convention is used to describe the properties of the various regions, see also Fig. 1.1. In this scope five different regions are identified. First the inner gas filled tube is sectioned into three parts, the rear section of the WGTS (rear), center of the WGTS (center) and front of the WGTS (front). Secondly the interfaces of gas and containment are named. So there is the beam tube which surrounds the gas cylindrically (tube) and the so called rear wall (RW) at the rear end of the WGTS.

In general there are 3 different types of electrons, two types of ions and one type of neutral particles. They are mainly distinguished by their energy density distribution. There are thermal electrons (e,th), following the Maxwell-Boltzmann-distribution, β electrons (e,β) following the Fermi-distribution and high energy electrons (e,he) not following either of both distributions. The ions are described by a part which follows the Maxwell-Boltzmann-distribution (i,th) and a part that follows some other unspecified energy distribution. Lastly there are neutral particles (n) which are not distinguished into their energy distribution.

For these particle types some properties are of importance: the number density n, the current density j and the velocity v.

In addition the system has some other characteristics: the potential U, the electric fields E and the magnetic fields B.

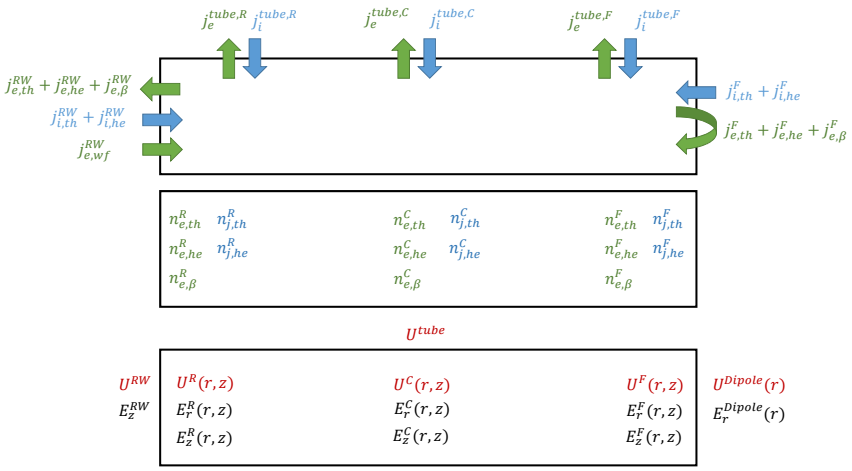


Figure 1.1: Sketch of relevant parameters. The arrows indicate the current, not necessarily the particle flow direction ($j = q \cdot n \cdot v$).

2 Available and future simulations

This chapter comprises an incomplete list of simulations used in the plasma and ion business

2.1 Monte Carlo simulations for the electron spectrum

What does it do? Calculate the electron spectrum of primary and secondary electrons using the Monte Carlo technique

Physical processes Injection of primary electrons, ionisation, elastic scattering, unconfirmed list of other processes

Input into the model Ion fluxes (or ion creation rates respectively), electric field (from plasma simulations), gas flow rates, electron-hydrogen cross sections

A priori assumptions The time a particle spends inside the WGTS is proportional to its energy.

Validation No validation is known

Output Equilibrium electron spectrum integrated over the whole beam tube (shown in Fig. 2.1)

2.2 Plasma simulation (Laura)

What does it do? Calculate the plasma potential

Physical processes Electron diffusion, plasma wall interaction

Input into the model Ion fluxes (or ion creation rates respectively), gas flow rates, work function of the boundary material

A priori assumptions Plasma is purely thermal, electrons are behaving diffusive

Validation No validation is known

Output Equilibrium plasma potential for various rear-wall voltages

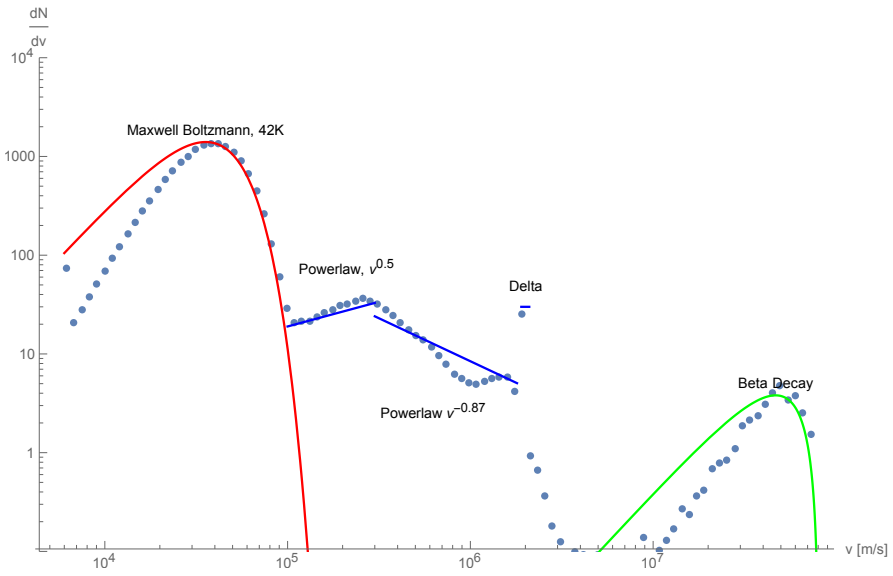


Figure 2.1: Output of the Monte Carlo simulations. The dotted results are fitted with the three components (Maxwell-Boltzmann, broken power-law and Fermi spectrum) plotted with solid lines.

3 Experimental data and its modelling

3.1 Currents

3.1.1 Rear wall

The rear wall is not electrically connected to the rest of the beam tube and may be biased with the voltage U^{RW} (cf. Fig. 3.1). The current between the rear wall and ground can be measured.

From a plasma physical viewpoint the situation may be best described as similar to a Langmuir probe. A very simplified on the typical current-voltage diagram of a Langmuir probe is given in Fig. 3.2.

The main result of the measurement at 50% column density is depicted in Fig. 3.3 The measured quantities are: the rear wall current $j^{\mathrm{RW}}_{\mathrm{total}}$ and the ion current at the dipoles $j^{\mathrm{dipole}}_{\mathrm{i}}$ in dependence of the rear wall voltage U^{RW}. In order to understand the current $j^{\mathrm{RW}}_{\mathrm{total}}$ we identified the various contributions to the current:

- $j^{\mathrm{RW}}_{\mathrm{e,th}}$ current from thermal electrons
- $j^{\mathrm{RW}}_{\mathrm{i,th}}$ current from thermal ions
- $j^{\mathrm{RW}}_{\mathrm{e,he}}$ current from high-energy electrons (non-thermalized electrons), no primary β electrons
- $j^{\mathrm{RW}}_{\mathrm{e},\beta}$ current from unscattered β electrons
- $j^{\mathrm{RW}}_{\mathrm{i,he}}$ current from high-energy ions (all ions above 1eV kinetic energy, manly from dissociation)
- $j^{\mathrm{RW}}_{\mathrm{e,wf}}$ current from emission from the rear wall (from plasma theory of Langmuir probes)

So the total current at the rear wall is given by

$$j^{\mathrm{RW}}_{\mathrm{total}} = j^{\mathrm{RW}}_{\mathrm{e,th}} + j^{\mathrm{RW}}_{\mathrm{e,he}} + j^{\mathrm{RW}}_{\mathrm{e},\beta} + j^{\mathrm{RW}}_{\mathrm{e,wf}} + j^{\mathrm{RW}}_{\mathrm{i,th}} + j^{\mathrm{RW}}_{\mathrm{i,he}} \tag{3.1}$$

The current was measured for different rear wall potentials. Here we focus on the saturation value $U^{\mathrm{RW}}_{-} = -1\,\mathrm{V}$ and $U^{\mathrm{RW}}_{+} = 5\,\mathrm{V}$ (personal communication, 2019/03/12, Magnus Schlösser, measurement with broader rear wall potential setting than presented in 3.3). The total current at the rear wall reads to $j^{\mathrm{RW}}_{\mathrm{total}}(U^{\mathrm{RW}}_{-}) = 8\,\mathrm{nA}$ and $j^{\mathrm{RW}}_{\mathrm{total}}(U^{\mathrm{RW}}_{+}) = 80\,\mathrm{nA}$. The current is 9 times higher for positive voltages than for negative voltages.

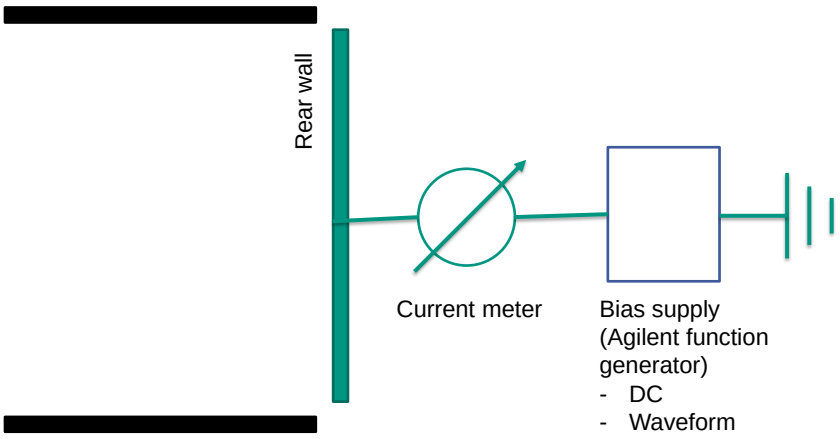


Figure 3.1: Schematic of the rear wall

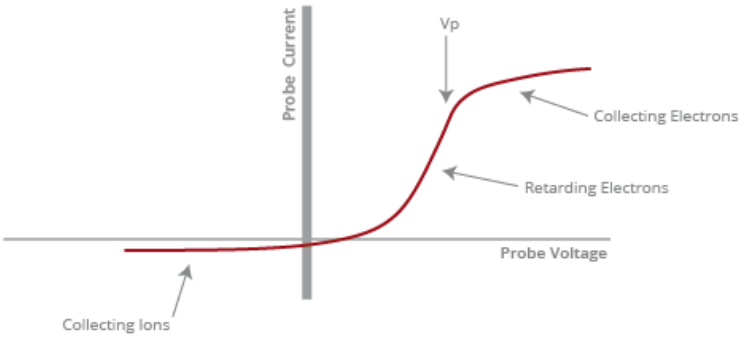


Figure 3.2: Sketch of the U-I-diagram for a Langmuir probe. Stolen from the friendly people at Impedans Ltd.

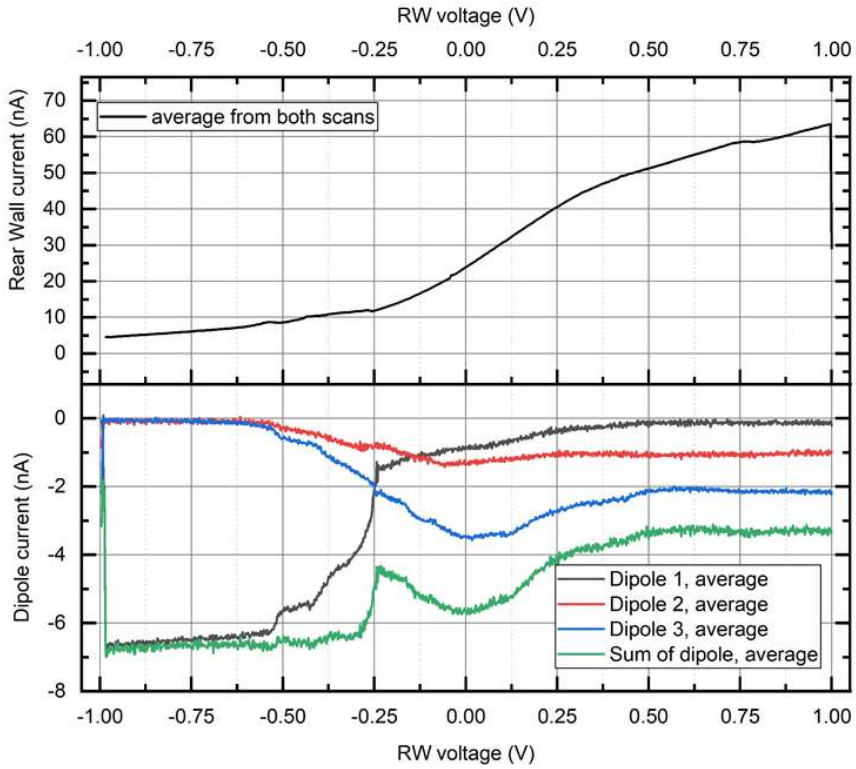


Figure 3.3: Rear wall current (upper panel) and dipole current (lower panel) vs. Rear wall voltage at 50% column density. The plot with bigger voltage range will be included as soon as it is available

Assumption 1: The contribution j_{wf} may be safely ignored as the rear wall is at very low temperatures. So no electrons are emitted from the rear wall.

Assumption 2: The thermal current of electrons $j_{\mathrm{e,th}}^{\mathrm{RW}}$ is zero at large negative values (Boltzmann-distribution around 2 meV) and the current of the thermal ions $j_{\mathrm{i,th}}^{\mathrm{RW}}$ is zero at large positive values (Boltzmann-distribution around 2 meV).

This leads to the two following cases:

$$j^{\mathrm{RW}}(U_{+}^{\mathrm{RW}}) = j_{\mathrm{e,th}} + j_{\mathrm{e,he}} + j_{\mathrm{e},\beta} + j_{\mathrm{i,he}} \tag{3.2}$$

$$j^{\mathrm{RW}}(U_{-}^{\mathrm{RW}}) = j_{\mathrm{e,he}} + j_{\mathrm{e},\beta} + j_{\mathrm{i,he}} + j_{\mathrm{i,th}} \tag{3.3}$$

Assumption 3: The high energy, and β current are independent of the rear wall voltage. So the measurement results can be written as

$$j^{\mathrm{RW}}(U_{+}^{\mathrm{RW}}) = 9 \cdot j^{\mathrm{RW}}(U_{-}^{\mathrm{RW}}) \tag{3.4}$$

$$j_{\mathrm{e,th}} + j_{\mathrm{e,he}} + j_{\mathrm{e},\beta} + j_{\mathrm{i,he}} = 9 \cdot (j_{\mathrm{e,he}} + j_{\mathrm{e},\beta} + j_{\mathrm{i,he}} + j_{\mathrm{i,th}}) \tag{3.5}$$

$$\Rightarrow j_{\mathrm{e,th}} = 8 \cdot (j_{\mathrm{e,he}} + j_{\mathrm{e},\beta} + j_{\mathrm{i,he}}) + 9 \cdot j_{\mathrm{i,th}} \tag{3.6}$$

Assumption 4: The energy density distribution of electrons is given as depicted in Fig. 2.1 from Ferencs simulation.

Assumption 5: According to Ferenc (personal communication, 2019/03/12) the blue part of the spectrum will vanish due to thermalization and lack of gas to produce new secondaries and only the red and green part will remain. So we can assume $j_{\mathrm{e,he}}^{\mathrm{RW}} = 0$

With assumption 4 we can calculate the currents for each electron species s by using

$$j_{\mathrm{s}} = q_{\mathrm{s}} \cdot \int v \frac{dn_{\mathrm{s}}}{dv} dv \tag{3.7}$$

If we also use assumption 5 we can compare the currents of the red (thermal) part and of the green (β) part of the spectrum. A simple integration with Mathematica over the fits yields $j_{\mathrm{e,th}}/j_{\mathrm{e},\beta} = 3.7 \times 10^{-4}$. With both assumptions 4 and 5 we can rewrite Eq. 3.6 to

$$\frac{8 j_{\mathrm{e},\beta}}{j_{\mathrm{e,th}}} = \frac{-8 j_{\mathrm{i,he}} - 9 j_{\mathrm{i,th}}}{j_{\mathrm{e,th}}} \tag{3.8}$$

$$\frac{8}{3.7 \cdot 10^4} = \frac{-8 j_{\mathrm{i,he}} - 9 j_{\mathrm{i,th}}}{j_{\mathrm{e,th}}} \tag{3.9}$$

$$20000 \cdot j_{\mathrm{e,th}} = -8 j_{\mathrm{i,he}} - 9 j_{\mathrm{i,th}} \tag{3.10}$$

So we see that the thermal electron current has to be a lot smaller than the total ion current.

From here on we have to add an assumption for the ion currents. On the one hand we can assume that the number density of the thermal ions and the thermal electrons are comparable or on the other hand we assume that the ion currents at both ends of the WGTS is equal in distribution and value.
At first we discuss the first assumption: If the number densities of the thermal electrons and thermal ions are comparable we can extract the thermal ion current as shown in the following

$$j_{\mathrm{i,th}} \approx -\frac{1}{\sqrt{\frac{m_i}{m_e}}} j_{\mathrm{e,th}} \approx -\frac{1}{70} j_{\mathrm{e,th}} \tag{3.11}$$

With Eq. 3.10 we get then for the high energy electron current

$$j_{\mathrm{i,he}} \approx 2421 j_{\mathrm{e,th}} \tag{3.12}$$

This would in turn mean, that the high energy current is much higher than assumed right now.

Secondly we discuss the case where the ion current at both sides of the WGTS is equal in distribution and value:

Assumption 6: The current of ions leaving the WGTS at both ends are of the same order. ($j_{\mathrm{i,total}}^{\mathrm{RW}} \approx j_{\mathrm{i,total}}^{\mathrm{dipole}}$)

From the measurement (see Fig. 3.3) we get a mean value of the ion current at the dipoles of $j_{\mathrm{i,total}}^{\mathrm{dipoles}} \approx -5\,\mathrm{nA}$. With assumption 6 and the measured ion current we can modify Eq. 3.10. So we get

$$j_{\mathrm{e,th}}^{\mathrm{RW}} \approx \frac{1}{20000} \cdot j_{\mathrm{i,total}}^{\mathrm{dipole}} \tag{3.13}$$

$$j_{\mathrm{e},\beta}^{\mathrm{RW}} \approx \frac{1}{3.7 \cdot 10^{-4}} j_{\mathrm{e,th}}^{\mathrm{RW}} \tag{3.14}$$

$$\Rightarrow j_{\mathrm{e},\beta}^{\mathrm{RW}} \approx 0.9\,\mathrm{nA} \tag{3.15}$$

With 50% column density an activity of 10^{11} Bq is expected, which translates into a current of 8 nA of primary β electrons. So we see that there are 7 nA of current left, which are not accounted for in this calculation.

We see that the current measured at the rear wall can not be explained with the model presented above. This means that at least one of the assumptions 1-6 are not true. So here we take a closer look into those assumptions. Assumption 2 and assumption 3 seem to be most reasonable. If assumption 2 is wrong the ion retention method would not work (it is based on electrostatic repulsion). Same is true for the high energy electrons. They are not heavily influenced by the rear wall potential (KATRIN would not work if this would be the case). So only assumptions 1,4,5 and 6 are under investigation. If

assumption 6 is wrong there has to be a new mechanic to heavily influence ions on both sides of the WGTS differently. As of yet this special mechanic has not been identified. At this point we encourage to read section 3.1.2. Assumptions 1,4,5 are closely related. So if assumption 1 is wrong assumption 4 and 5 have to be wrong as well, because this effect was not included in the simulations.
At this point it is highly likely that assumption 4 and 5 are wrong. Concluding that the energy density distribution of the electrons at the rear wall can not be described by the simulation of sec. 2.1. It is very likely that there exists a non-negligible part of high-energy electrons, which are no primary β electrons.

Fast approximation of the rear wall current

Here we present a fast method to calculate the currents at the rear wall. This can only be seen as a rough estimation of the underlining effects. The calculation differ from the calculation presented above in the determination of the current from the energy distribution.
We start similar to the calculation above with the measurement of the rear wall current. The total current at the rear wall reads to $j^{\mathrm{RW}}_{\mathrm{total}}(U^{\mathrm{RW}}_{-}) = 8\,\mathrm{nA}$ and $j^{\mathrm{RW}}_{\mathrm{total}}(U^{\mathrm{RW}}_{+}) = 80\,\mathrm{nA}$. So the current is 9 times higher for positive voltages than for negative voltages. We assume that the current for large positive values of the rear wall potential blocks all ions. Additionally we neglect the ion current from this point on, because it will only increase the effect shown below. So we start from:

$$j^{\mathrm{RW}}_{\mathrm{e,th}} = 9 j^{\mathrm{RW}}_{\mathrm{e},\beta} \tag{3.16}$$

Here we use that the mean current can be calculated by $j = q \cdot n \cdot v$ and that the mean velocities can be calculated from their mean energy. The mean energies are: $E_{\mathrm{e,th}} = 5\,\mathrm{meV}$ and $E_{\mathrm{e},\beta} = 5\,\mathrm{keV}$ respectively. This translates into $v_{\mathrm{e},\beta} = 1000 v_{\mathrm{e,th}}$. So we can derive a formula for the densities of the thermal and β electrons.

$$n_{\mathrm{e,th}} v_{\mathrm{e,th}} = 9 \cdot n_{\mathrm{e},\beta} v_{\mathrm{e},\beta} \tag{3.17}$$

$$\frac{n_{\mathrm{e,th}}}{n_{\mathrm{e},\beta}} = 9 \frac{v_{\mathrm{e},\beta}}{v_{\mathrm{e,th}}} \tag{3.18}$$

$$\frac{n_{\mathrm{e,th}}}{n_{\mathrm{e},\beta}} = 9000 \tag{3.19}$$

Under the assumption that the velocities are correct and that the high-energy current is solely made up of primary electrons we find that the density of thermal electrons has to be round about 9000 times higher than the non-thermal electron density.

This prediction may then be compared to Fig. 2.1. According to Ferenc (personal communication, 2019/03/12) the blue part of the spectrum will vanish due to thermalization and lack of gas to produce new secondaries and only the red and green part will remain. As the spectrum is a differential velocity spectrum, the density can be calculated by integrating over the velocity $n = \int_0^\infty dN/dvdv$. We may identify the following components $n_{\mathrm{e},\beta} = \int_{\mathrm{green}} dN/dvdv$ and $n_{\mathrm{e,th}} = \int_{\mathrm{red}} dN/dv\,dv$. A simple integration with Mathematica over the fits yields $n_{\mathrm{e,th}} = 4.2 n_{\mathrm{e},\beta}$. This is significantly different from 9000.

So one of the following assumptions must be wrong:

1. The secondary, non-thermal electrons are negligible or non-existent
2. The velocities of the electrons are as given above
3. The electron spectrum is exactly as given in Fig. 2.1

The first assumption can be tested by calculating the current by using $j = e \int_0^\infty v dN/dv dv$ which is essentially the first moment of the distribution function. Here the contribution of the *blue* part of the spectrum can be compared to the red part. While the non-thermal secondaries are not as numerous as the thermal electrons they still have a significantly higher velocity resulting in a massively higher current.

In the following the integrals $n_{\text{red}}, n_{\text{blue}}, n_{\text{green}}$ for the densities (the naming follows the colouring of the graph) and the respective current integrals $j_{\text{red}}, j_{\text{blue}}, j_{\text{green}}$.

It can easily be shown that $n_{\text{red}}/n_{\text{green}} = 4.1$ which is much less than the desired value of 9000. Even if all secondaries will eventually cool down the number of electrons is still $(n_{\text{red}} + n_{\text{blue}})/n_{\text{green}} = 4.1$ [1] This in turn means, that there are not enough thermal electrons present to explain the measured current.

If one calculates the currents $j_{\text{red}}/j_{\text{green}} = 3.7 \times 10^{-4}$. So in fact the factor of 9000 is wrong by a factor of 3 [2]. But this is still well below any current needed to explain the measurements.

The ratio $j_{\text{blue}}/j_{\text{red}}$ however is approx. 200, i.e., the contribution of secondary, non-thermal particles to the total current is well above the contribution of thermalized secondaries.

Still the contribution of all secondaries reaches only 0.08 of the primary contribution, but it is clear that thermalized electrons cannot be the source of the missing current. The large uncertainties of the secondary, non-thermal spectrum leave plenty of room for improvement (e.g., the current associated with the delta spike at $v = 2 \cdot 10^6$ m/s is not considered).

3.1.2 Dipole section

The dipole section is fitted with a number of dipoles that can block ions from entering the spectrometer. The general idea is that all particles enter the dipole section, ions are blocked and electrons are reflected in the spectrometer. A sketch is given in Fig. 3.4.

It is a general belief that all charged particles within the WGTS are strictly bound to magnetic field line which are strictly aligned parallel to the beam tube. A consequence of this concept is, that charges will hit either end of the beam tube or has to accumulate within the beam tube.

The current has been measured. The main result is depicted in Fig. 3.3. Two points have to be noted:

[1] All values here are normalized to the "green" (i.e., primary tritium decay electron) densities and currents to avoid lengthy calculations.

[2] This is mostly due to the fact, that there many electrons in the Maxwell distribution with velocities well above the thermal mean velocity.

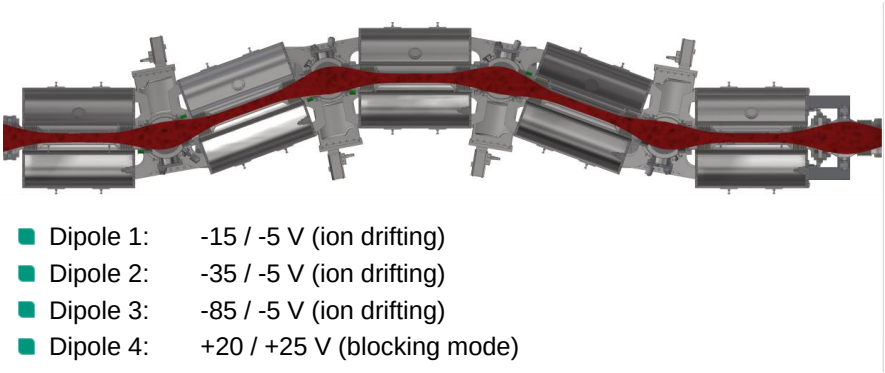


Figure 3.4: Schematic of the dipole section.

1. There is an equilibrium current

2. The equilibrium current is opposite to and smaller than the rear wall current

From the first point it can be safely assumed that the beam tube is not constantly charging up. In conjunction with the second finding it becomes clear that charges may end up somewhere else than one of the both ends of the beam tube.

In first place one has to clarify that ionisation and recombination processes do not play a role in this question: Any recombination process will diminish the ion current, but also the electron current on the other side of the beam tube.

Now a loss mechanism has to be found that allows the deflection of ions to the wall of the beam tube. This requires a process that may move ions away from their magnetic field lines. Two ideas have been discussed:

- Ions are coupled to the gas flow in the center of the beam tube (where we find high gas densities). At that point the possibility of pumping out along with the gas should be considered. This includes that the ions hit the tube wall and are neutralized. The question here is: How large is the possible deflection from ion-neutral collisions? Is the deflection larger than the bonding to the magnetic field line?

- The other possibility is a deflection near the dipoles: The gas density is sharply decreasing, but according to the Laura-simulations an electric field exists, that may help in deflecting the ions.

To check both possibilities it is necessary to quantitatively analyse the ion motion in the crossfire of magnetic field, neutral collision and electric field.

The sheer existence of a sizeable ion loss mechanism is a larger threat for the Laura-simulations: These build on ion creation rates (as basis for charge calculations). When ions go lost in a larger fraction, the calculation of the electric field may be significantly wrong.